Am J Transl Res 2026;18(6):5000-5014
www.ajtr.org /ISSN:1943-8141/AJTR0169168

Original Article

Diosgenin mitigates laser-induced choroidal neovascularization by suppressing the endothelial-to-mesenchymal transition via the TGF-β/Smad and MAPKs signaling pathways

Siqi Zhou[1*], Ning Yang[1*], Mengqi Gao[1], Fei Li[1], Caijian Xiong[1], Qinyi Hui[1], Yingxue Hu[1], Siqi Feng[1], Yan Shao[2], Xin Zhou[1], Qingzi Jin[1], Xinrong Xu[1]

[1]Department of Ophthalmology, Affiliated Hospital of Nanjing University of Chinese Medicine, Nanjing 210029, Jiangsu, China; [2]Department of Ophthalmology, Liyang Hospital of Chinese Medicine, Liyang 213300, Jiangsu, China. [*]Equal contributors.

Received October 7, 2025; Accepted May 26, 2026; Epub June 15, 2026; Published June 30, 2026

Abstract: Objectives: To explore whether diosgenin (Dio), a natural steroidal saponin, alleviates laser-induced choroidal neovascularization (CNV) and its underlying mechanism related to endothelial to mesenchymal transition (EndMT) and signaling pathways. Methods: A mouse model of laser-induced CNV was established; mice were treated with Dio (50 μM, 100 μM) or ranibizumab. In vitro, human umbilical vein endothelial cells (HUVECs) were stimulated with oxidized low-density lipoprotein (Ox-LDL) and pretreated with Dio. CNV leakage, lesion size, EndMT markers, and TGF-β/Smad and MAPKs pathway activities were detected by fundus angiography, Western blot, Transwell, and tube formation assays. Results: Dio reduced CNV leakage and lesion area in mice, inhibited HUVEC migration and tube formation. It downregulated mesenchymal markers (α-SMA, vimentin), upregulated endothelial markers (VE-cadherin, ZO-1), and suppressed phosphorylation of Smad2/3, p38, ERK1/2, and JNK. Conclusions: Dio mitigates laser-induced CNV by inhibiting EndMT via the TGF-β/Smad and MAPKs signaling pathways, serving as a potential candidate for neovascular age-related macular degeneration.

Keywords: CNV, diosgenin, endothelial-to-mesenchymal transition, TGF-β/Smad signaling pathway, MAPKs signaling pathway

Introduction

Diosgenin (Dio), a steroidal saponin derived from plants such as yam, fenugreek and citrus, has gained attention for its wide range of therapeutic effects, including the management of diabetes and its complications [1], the alleviation of neuroinflammation [2], and the treatment of psoriasis [3], among other conditions. Dio exerts its benefits through multiple biological mechanisms, which include reducing lipid and cholesterol levels [4], exhibiting anti-inflammatory effects [5, 6], scavenging free radicals through antioxidant actions [7], suppressing tumor growth [8], and providing protection against fibrosis [9].

Age-related macular degeneration (AMD) is the primary reason for irreversible blindness among older adults globally [10], which is clinically classified into early and late stages. Late-stage AMD manifests in two forms: dry AMD, distinguished by geographic atrophy (GA), and wet AMD, distinguished by choroidal neovascularization (CNV) [11]. CNV involves abnormal blood vessel growth from choroidal capillaries, which are prone to rupture, leakage and hemorrhage, damaging the macula - a region responsible for central vision [12]. As a result, CNV often leads to significant vision impairments and eventual blindness. Anti-VEGF therapies are a standard treatment for managing CNV in AMD [13]. However, the long-term nature, high costs and potential post-injection inflammation have caused concerns among some patients. The poor responses to anti-VEGF treatment in patients with nAMD are linked to subretinal fibrosis [14]. Additionally, repeated anti-VEGF

https://doi.org/10.62347/NCGU7615

injections may worsen geographic atrophy, complicating AMD management [15]. These circumstances underscore the necessity of seeking alternative therapies for CNV.

Recent research has emphasized the crucial contribution of EndMT in CNV progression [16-20]. Upon being stressed with inflammation, oxidative stress or hypoxia, endothelial cells undergo a radical change and shed their natural cell polarity to become mesenchymal cells. Newly-formed mesenchymal cells obtain distinct properties like increased proliferation, migration and invasiveness [21]. EndMT can result in the disruption of cytoskeletons [22], allowing choroidal endothelial cells to proliferate and migrate outwards along the extracellular matrix, ultimately leading to the formation of new blood vessels. Existing research findings suggest that inhibiting EndMT may effectively halt the progression of CNV.

TGF-β is involved in the regulation of cell proliferation and differentiation, with TGF-β1 playing a crucial role in angiogenesis and fibrosis [23-26]. Its signaling pathways are multifaceted, including the canonical Smad-dependent pathway and diverse Smad-independent pathways. Among numerous Smad-independent pathways, the MAPKs pathways are widely known, including the ERK, JNK and P38 signaling pathways, which are essential for cellular responses to TGF-β1 [27]. Studies have indicated that TGF-β stimulates VEGF release, induces ECM degradation, and increases vascular permeability [28-30]. During EndMT, it has been demonstrated that the TGF-β/Smad and MAPKs pathways play important regulatory roles [31]. TGF-β1 promotes EndMT in breast cancer stem-like cells (BCSLCs) by increasing Smad2/3 phosphorylation [32]. Jinzhao He discovered that the MAPKs signaling pathways were involved in the EndMT of bovine aortic endothelial cells (BAECs) mediated by homocysteine (Hcy) [33].

Recent research has demonstrated that Dio can mitigate myocardial fibrosis by counteracting the EndMT induced by ATO in HAECs [34]. Additionally, Dio has been found to possess anti-inflammatory properties by suppressing the LPS-induced translocation of NF-κB to the nucleus of HaCaT cells, and can partially suppress angiogenesis by downregulating VEGF-α expression in keratinocytes [3]. However, despite these promising findings, the potential relationship between Dio and CNV remains unexplored. Therefore, this study was designed to evaluate the therapeutic promise of Dio and its underlying mechanisms of laser-stimulated CNV.

Materials and methods

Reagents, drugs and antibodies

Diosgenin (MUST-1432180) was obtained from Manchester Biotechnology Ltd. (Sichuan, China) Ranibizumab was obtained from Jiangsu Province Hospital of TCM (Nanjing, China). Ox-LDL (YB-002) was acquired from Mohan Biotechnology Co., Ltd. (Shanghai, China) Collagen Type I monoclonal antibody (Ig-66761-1) was sourced from Proteintech (Wuhan, China). VEGF antibody (GTX21316) was bought from GeneTex Group (TX, USA). Various antibodies and conjugates were supplied by Abcam (Cambridge, UK), including goat anti-mouse IgG (ab150113), goat anti-rabbit IgG (ab150078), goat anti-rabbit IgG (HRP, ab6721) and so on. The antibodies used included anti-CD31 (ab9498), anti-α-SMA (ab7817), anti-vimentin (ab20346), anti-VE-cadherin (ab318152), anti-ZO-1 (ab307799), anti-Smad2/3 (ab202445), anti-p-p38 (ab195049) and anti-p38 (ab170-099) and so on.

Animals

Male C57BL/6J mice (~6 w, 20-25 g) were obtained from Sibeifu Biotechnology Co., Ltd. located in Suzhou, China. The animals were provided with humane care in compliance with guidelines of the Association for Vision and Ophthalmic Research for animal use in research. All procedures performed under IACUC protocol, with an approval number of 2023NL-KS183.

Mouse model with laser-induced CNV

The methodologies for establishing animal models followed previous reports [16]. Mice were first dilated with 1% tropicamide (Santen, Japan) and then anesthetized through the intraperitoneal injection of Avertin (Sigma, USA) at a dose of 0.2 ml/10 g. A krypton laser with a wavelength of 577 nm was used for modeling. Key parameters included a spot diameter of 100 μm, a power output of 150 mW, and an

exposure duration of 0.1 second. Photocoagulation was performed around the optic disc of each mouse, at a distance of 2-4 PD, with a total of five spots treated in each eye.

Animal grouping and administration

Fifty mice were randomly assigned to five groups: normal, model, ranibizumab, 50 μM diosgenin (Dio50) and 100 μM diosgenin (Dio100). The normal group received no intervention. Starting on the second day after laser treatment, the model group was given a daily intraperitoneal injection of 0.1% DMSO. Dio was dissolved in 0.1% DMSO and prepared as solutions with concentrations of 50 μM and 100 μM, which were administered intraperitoneally once daily for two weeks. Mice in the ranibizumab group received a single intravitreal injection of 1 μL of ranibizumab on the second day after laser treatment.

Fundus photography

Fourteen days after laser treatment, all mice were first anesthetized and then dilated. Sodium hyaluronate was used as a viscoelastic agent to prepare the ocular surface. A clean glass slide was placed over the viscoelastic agent to flatten the cornea, followed by positioning a 120D biomicroscopy lens in front of the mice's eyes. Fundus imaging was performed using a fundus camera (CANON, Tokyo, Japan) to capture retinal images of the mice.

Optical coherence tomography

At 14 days post-laser induction, animals underwent standardized anesthesia and were then dilated. Sodium hyaluronate was used as a viscoelastic agent to prepare the ocular surface. A clean glass slide was placed over the viscoelastic agent to flatten the cornea, followed by positioning a 120D biomicroscopy lens in front of the mice's eyes. Optical phase tomography imaging of the mouse fundus was performed using an OCT machine (ZEISS, Oberkochen, Germany).

Fluorescein angiography

Fourteen days after laser treatment, fluorescein angiography (FA) was performed using a TOPCON fundus camera (Tokyo, Japan). Prior to imaging, all the mice underwent anesthesia, with their pupils dilated. A 0.05 mL intraperitoneal injection of 10% fluorescein sodium was administered, and retinal images were captured at both early (< 2 minutes) and late (> 7 minutes) stages after injection. The fluorescence intensity of the lesions was measured and analyzed using the ImageJ software. The lesions were categorized according to a standardized grading system [35]: Level 0: Weak high fluorescence or spot fluorescence with no leakage; Level 1: High fluorescence lesions with no gradual increase in either size or intensity; Level 2: increased fluorescence intensity without an increase in size; Level 3: Pathological lesions with increased fluorescence intensity and size.

Immunostaining of RPE-choroidal flat mount

Fourteen days after laser treatment, the mice were anesthetized and underwent cardiac perfusion. Once their tails became fully stiff, their eyeballs were excised and immersed in 4% PFA for 2 hours. A systematic dissection protocol was implemented to isolate the cornea, iris, and crystalline lens with surgical precision. The retinal neurosensory layer was gently removed using a brush, and the sclera was carefully peeled away and evenly cut around the periphery. The eyes were then flattened into a petal-like shape. Each flat mount was treated with 50 μL of diluted primary antibodies for collagen I (1:500) and VEGF (1:250) and incubated overnight at 4°C. After washing, the mounts were incubated in 50 μL of fluorescent secondary antibody diluted at a ratio of 1:500 for 30 minutes. Laser lesions were then analyzed using confocal microscopy (Leica Microsystems, Germany). ImageJ (NIH, version 1.8.0) software was used to quantify regions positive for collagen I and VEGF.

Cell culture and treatments

HUVECs were sourced from ATCC, grown in ECM (Procell, Wuhan, China), enriched with 10% FBS, 1% P/S and 6.67 μmol/L heparin to promote the optimal cell growth. The culture was maintained at 37°C in a 5% CO_2 incubator to simulate endothelial cell conditions. Before treatment with Ox-LDL (50 μg/mL) to induce endothelial dysfunctions, cells were pretreated with Dio at various concentrations including 10 μM, 20 μM and 40 μM (Dio10, Dio20, Dio40)

for 12 hours, allowing for a sufficient Dio uptake prior to Ox-LDL exposure.

Transwell assay

The experimental procedure closely followed the methodologies described in previous studies [16]. A modified Boyden chamber migration assay was performed in a 24-well format (Corning, NY, USA). HUVECs were resuspended at a density of 1×10^5 cells/mL in the upper chambers, which contained 200 μL of DMEM. The lower chambers were loaded with 500 μL of DMEM containing 10% fetal bovine serum and cultured for 24 h. Non-migrated cells were discarded, while the migrated ones were fixed, stained and rinsed. Following three washes with PBS, the average cell migration count across five distinct microscope fields was calculated by three researchers (CKX31, Olympus, Tokyo).

Tube formation assay

The experimental procedure closely followed the methodologies described in previous studies [16]. A 96-well plate was covered with 50 μL of matrix (Corning, New York, USA). HUVECs (2×10^4 cells) were plated in the matrix gel and incubated at 37°C for 10 to 16 hours. Blood vessel formation was observed in each cell group and photographed using an Olympus CKX31 microscope (Tokyo, Japan). The lengths of the formed tubular structures were quantified using an ImageJ angiogenesis analyzer (NIH, USA).

Cell immunofluorescence assay

The experimental procedure closely followed the methodologies described in previous studies [16]. According to established protocols, HUVECs from the designated groups were plated onto coverslips in 24-well plates. After rinsing twice with PBS, cells were fixed using 4% PFA for ten minutes. Subsequently, the samples were treated with 0.1% Triton X-100 in PBS for another 10 minutes. After blocking with 0.5% Triton X-100 containing 1% BSA for 30 minutes, cells were then treated with anti-CD31 (1 μg/ml) and anti-α-SMA (1 μg/ml) for 24 h at 4°C. Finally, the cells were exposed to a fluorescent secondary antibody (dilution ratio: 1:200) for 1 hour and stained with a DAPI solution for 5 minutes. Images were captured using an Olympus microscope (Tokyo, Japan).

Western blot

Proteins were extracted from retinal and choroidal tissues, as well as cell cultures, using a RIPA lysis buffer (Sigma Aldrich, MFCD 02100484), and its concentration was measured using the BCA method. A total of 30 μg of proteins were then denatured via boiling in water for 5 minutes, which were transferred onto a PVDF membrane using 10% SDS-PAGE and blocked with 10% BSA for 1 hour. The membrane was subsequently incubated overnight at 4°C with primary antibodies, including α-SMA, vimentin, VE-cadherin, ZO-1, TGF-β1, Smad2/3, p-Smad2, p-Smad3, p38, p-p38, ERK1/2, p-ERK1/2, JNK and p-JNK (all at a dilution ratio of 1:1000), and GAPDH (dilution ratio: 1:2000). Following additional washes, samples were treated with secondary antibodies (dilution ratio: 1:10,000) for 2 hours. Immunocomplexes were detected and visualized using an enhanced chemiluminescence detection kit. The intensity of the bands was measured using ImageJ (NIH, version 1.8.0) software.

Statistical analysis

All data presented is expressed as mean ± SD. Statistical analyses were performed using the GraphPad Prism version 8.0.1. Significance was determined through one-way ANOVA followed by a Dunnett's test, with a *P*-value < 0.05 considered statistically significant.

Results

Dio reduced the fluorescent leakage and suppressed the progression in modeled mice

To assess the therapeutic effects of Dio in CNV, OCT was employed to measure the size of CNV lesions 14 days after treatment. The OCT images from the model group revealed significant subretinal hyperreflective signals and fluid accumulation, both of which were hallmark indicators of active CNV. In contrast, the ranibizumab and Dio treatment groups showed dramatic reductions in these hyperreflective signals, and no fluid accumulation was observed in the treated eyes, suggesting that the treatment effectively reduced the pathological CNV devel-

opment (**Figure 1A**). Fourteen days after treatment, FA was conducted to assess the leakage of CNV. In the early phase of angiography, laser lesions in the model group exhibited high fluorescence that was intensified and expanded during the late phase (**Figure 1B**), indicating a grade-3 laser lesion. Compared to the proportion (54%) of grade-3 lesions in the model group, the proportions in the ranibizumab (15%), 50 μM Dio (46%) and 100 μM Dio groups (26%) were significantly reduced (**Figure 1C**). RPE-choroidal flat mounts with collagen I and VEGF antibodies were applied to assess the therapeutic effects of Dio in CNV mice (**Figure 1D**, **1E**). The areas of both fibrosis and CNV were significantly reduced in mice treated with ranibizumab, as well as in those receiving Dio with a concentration of 100 μM.

These findings suggest that Dio has potent therapeutic effect in inhibiting the progression of both CNV and fibrosis, positioning it as a promising candidate for the treatment of diseases associated with these pathological conditions.

Dio treatment inhibited EndMT in model mice with CNV

Considering the pivotal role of EndMT in CNV [16, 17], a Western blot analysis was carried out to assess the expression level of EndMT-related proteins, including α-SMA, vimentin, VE-cadherin and ZO-1, in RPE-choroidal tissues (**Figure 2A**). In the model mice, the protein levels of α-SMA and vimentin were significantly elevated, while the expression of VE-cadherin and ZO-1 was markedly reduced compared to that of control mice. However, following Dio treatment, the protein expression of these markers was partially reversed (**Figure 2B**). These findings indicate that Dio effectively inhibits EndMT in laser-induced CNV in mice. To confirm the causal relationship between Dio-mediated EndMT inhibition and CNV suppression, we performed α-SMA overexpression rescue experiments. Western blot results showed that the pcDNA-α-SMA vector significantly upregulated α-SMA expression in RPE-choroidal tissues compared with the empty vector control (Figure S1A, S1B, $P < 0.01$). Quantitative analysis of fluorescein angiography revealed that α-SMA overexpression completely reversed the inhibitory effect of Dio on CNV leakage: the proportion of grade-3 lesions in the pcDNA-α-SMA + Dio100 group was significantly higher than that in the Dio100 group (Figure S1C, $^{\&\&}P < 0.01$) and showed no significant difference from the Model group ($^{ns}P \geq 0.05$). These in vivo results indicated that α-SMA-mediated EndMT is a necessary target for Dio's anti-CNV effect.

Dio treatment reduced tissue expression of TGF-β/Smad and MAPKs pathways in model mice with CNV

Smad2/3 and MAPKs pathways are well-established regulators in TGF-β-induced angiogenesis [27], including endothelial cell survival, migration and proliferation, which are critical to the development of pathological vascularization, such as CNV [36]. On the other hand, following a comparative analysis of the protein expression profiles between the control and model groups, we observed a notable upregulation of p-Smad2, p-Smad3, p-p38, p-ERK1/2 and p-JNK within the model group, which directly corroborated the aberrant protein enrichment of the TGF-β/Smad and MAPKs pathways in CNV (**Figure 3A**). Notably, after administering Dio to a CNV model for a duration of two weeks, therapeutic intervention induced a marked reduction in protein phosphorylation relative to baseline measurements (as illustrated in **Figure 3B-D**, **3F-H**).

Dio suppressed the migration and lumen formation of Ox-LDL-induced HUVECs

It is well-established that cellular migration and tubulogenesis are crucial for the formation and extension of neovascularization, including those in the progression of choroidal neovascularization (CNV) [37, 38]. Therefore, to investigate the impact of Dio on angiogenesis, we established a cellular model of CNV by stimulating HUVECs with Ox-LDL. We further evaluated the functions of Dio on the migratory and tubulogenic capabilities of HUVECs using Transwell assays and a matrigel matrix. Experimental results demonstrated that, compared to the normal group, the number of migratory cells in the model group significantly increased. Notably, compared to the model group, treatment with Dio significantly inhibited the migration of HUVECs (**Figure 4A**, **4C**). On the other hand, compared to the normal group, the total tube length in the model group was significantly elongated. Importantly, after treatment with Dio, the total tube length markedly decreased

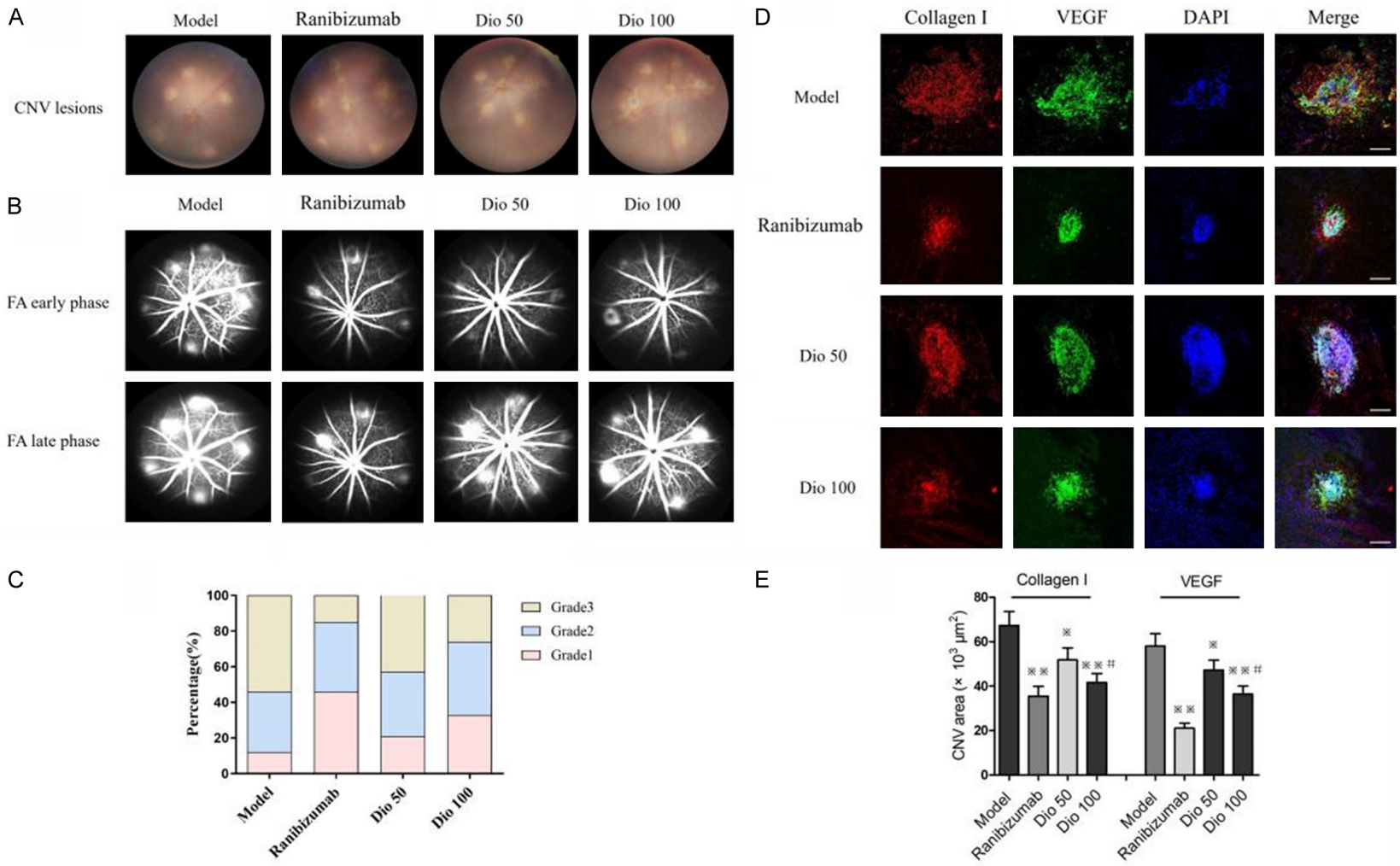

Figure 1. Dio reduced the fluorescent leakage and area of CNV in model mice. (A) Fundus photographs, and (B) Fluorescein angiography images of CNV in the model, ranibizumab, 50 μM Dio and 100 μM Dio groups respectively. (C) Histogram depicting the levels of leakage through angiography. The percentages of grade-3 laser lesions in each group. Data is expressed as mean ± S.D, n = 10. (D) RPE-choroidal flat mounts were prepared in each group, and representative images of fibrosis and CNV lesions were examined using collagen I and VEGF staining. (E) Quantification of collagen I and VEGF positive areas after two weeks of administration in each group. Data is expressed as mean ± S.D, n = 5. Scale bar = 100 μm. $^{*}P < 0.05$, $^{**}P < 0.01$ versus the model group, $^{\#}P < 0.05$ versus the ranibizumab group.

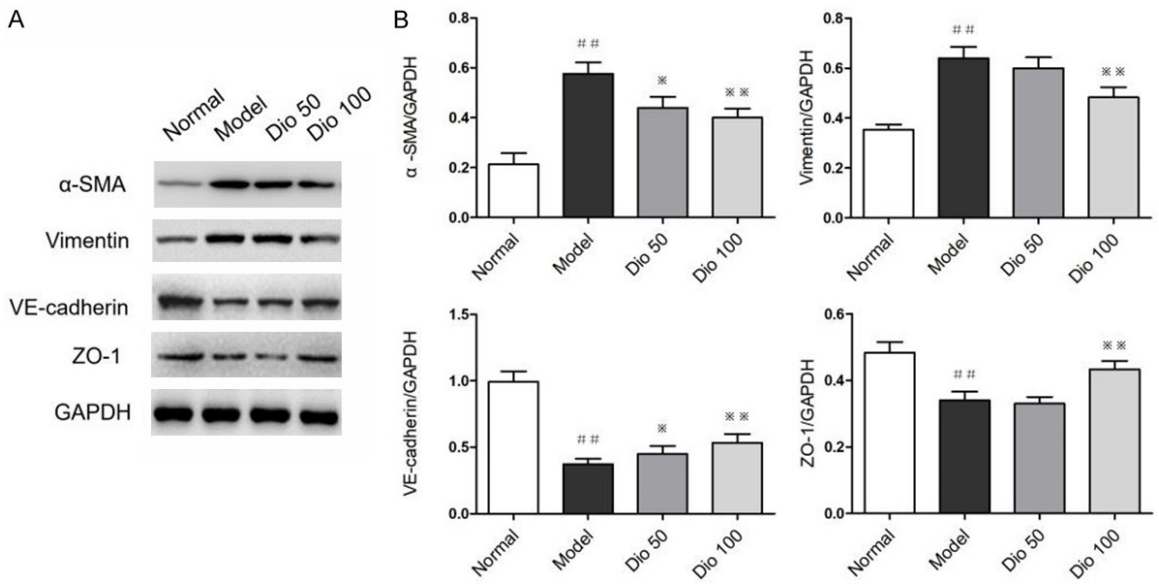

Figure 2. Dio treatment inhibited EndMT in model mice with CNV. A. Two weeks after administration, Western blot was used to evaluate the expression of α-SMA, vimentin, VE-cadherin and ZO-1 in the model, ranibizumab, 50 μM Dio and 100 μM Dio groups respectively. B. Quantification of α-SMA, vimentin, VE-cadherin and ZO-1 protein levels in each group. GAPDH was used as an internal control for protein equal loading. Data is expressed as mean ± S.D, n = 3. $^{**}P < 0.01$ versus the normal group; $^{\#}P < 0.05$, $^{\#\#}P < 0.01$, $^{ns}P \geq 0.05$ versus the model group.

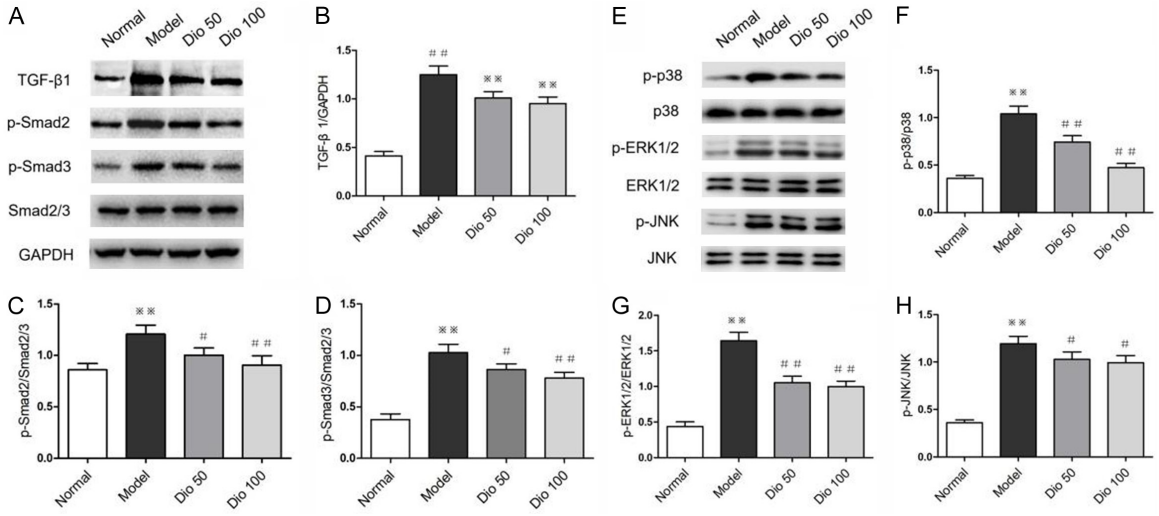

Figure 3. Dio treatment reduced the tissue expression of TGF-β/Smad and MAPKs pathways in model mice with CNV. A. Two weeks after administration, Western blot was used to evaluate the expression of TGF-β1, p-Smad2, p-Smad3 and Smad2/3 in the model, ranibizumab, 50 μM Dio and 100 μM Dio groups respectively. B-D. Quantification of TGF-β1, p-Smad2/Smad2/3 and p-Smad3/Smad2/3 protein levels in each group. E. Two weeks after administration, Western blot was used to evaluate the expression of p-p38, p38, p-ERK1/2, ERK1/2, p-JNK and JNK in each group. F-H. Quantification of p-p38/p38, p-ERK1/2/ERK1/2 and p-JNK/JNK protein levels in each group. GAPDH was used as an internal control for protein equal loading. Data is expressed as mean ± S.D, n = 3. $^{**}P < 0.01$ versus the normal group; $^{\#}P < 0.05$, $^{\#\#}P < 0.01$ versus the model group.

compared to that in the model group (**Figure 4B**, **4D**). Additionally, the effects of Dio on the migratory and tubulogenic capabilities of HUVECs were positively correlated with the concentration of Dio treatment, and this effects were not related to the toxicity of the drug to the cells themselves (Figure S3). These findings aligned with previous research, indicating that Dio exerted significant anti-angiogenic effects [39-41].

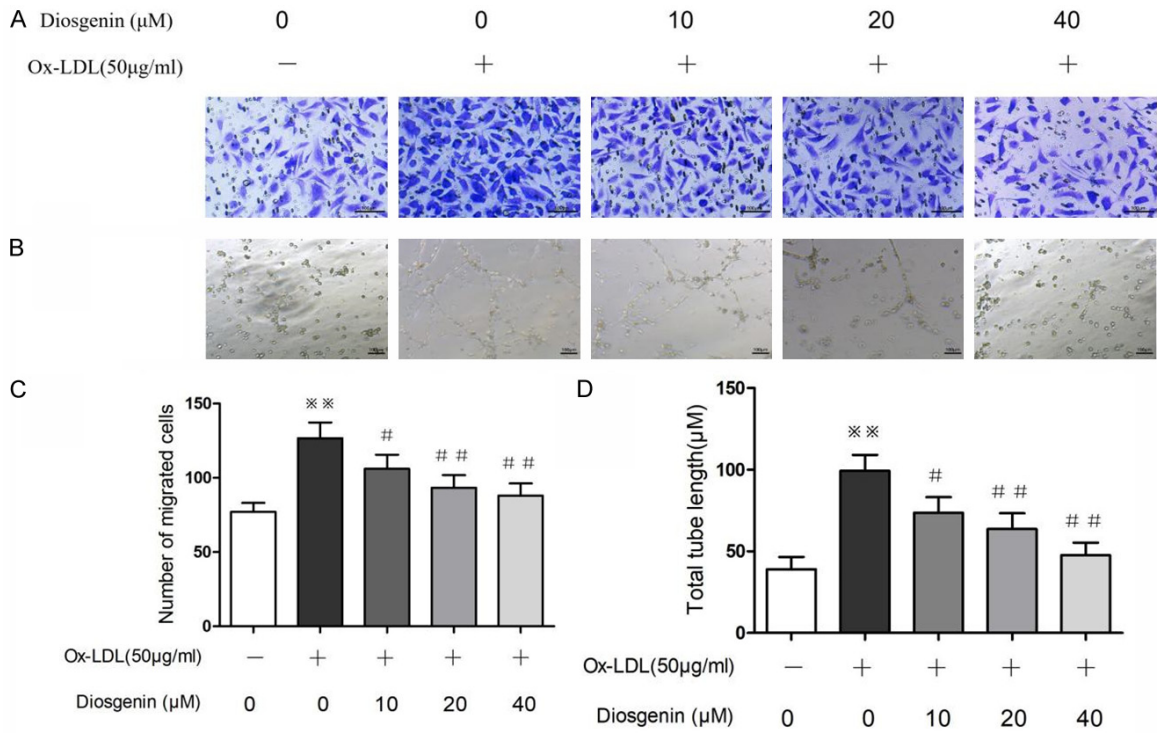

Figure 4. Dio inhibited cell migration and tube formation in HUVECs stimulated by Ox-LDL. Before Ox-LDL (50 μg/mL) stimulation, HUVECs were treated with 10, 20 and 40 μM Dio for 12 hours. (A) Cell migration was determined using a transwell assay, and (B) Tube formation was evaluated using a matrigel assay. (C, D) Quantify the number of migrating cells and tube length. Scale bar = 100 μm, Data is expressed as mean ± S.D, n = 3. $^{**}P < 0.01$ versus the normal group; $^{\#}P < 0.05$, $^{\#\#}P < 0.01$ versus the model group.

Dio prevented EndMT by inhibiting the TGF-β/Smad and MAPKs pathways in Ox-LDL-stimulated HUVECs

To estimate Dio's impact on EndMT in Ox-LDL-stimulated HUVECs, immunofluorescence staining was employed to quantify the expression levels of CD31 and α-SMA. Additionally, protein immunoblotting was utilized to quantify the protein abundance of α-SMA, vimentin, VE-cadherin and ZO-1. The immunofluorescence results revealed that Ox-LDL markedly reduced CD31 expression while concurrently increased α-SMA expression, indicating a transition towards a mesenchymal phenotype. Notably, these Ox-LDL-induced alterations were partially mitigated following pretreatment with Dio (**Figure 5A-C**). A Western blot analysis further confirmed that a 24-hour exposure to Ox-LDL resulted in upregulated α-SMA and vimentin, and downregulated ZO-1 and VE-cadherin. Intriguingly, pretreatment with Dio partially reversed these effects, with the most significant reversal observed at a Dio concentration of 40 μM (**Figure 5D**). Additionally, we further elucidate the mechanisms through which Dio modulated EndMT. Our results demonstrated a marked upregulation of TGF-β1, p-Smad2, p-Smad3, p-p38, p-ERK1/2 and p-JNK following 24-hour stimulation with Ox-LDL (**Figure 6A**, **6E**). Notably, pretreatment with Dio significantly attenuated these increases, with the most pronounced effect observed at a concentration of 40 μM (**Figure 6B-D**, **6F-H**). These findings suggest that Dio inhibits EndMT in Ox-LDL-stimulated HUVECs by the TGF-β/Smad and MAPKs signaling channels. Consistent with in vivo findings, in vitro experiments showed that α-SMA overexpression abrogated the inhibitory effect of Dio on the angiogenic capacity of HUVECs: the tube formation and cell migration abilities in the pcDNA-α-SMA + Dio40 group were significantly enhanced compared with the Dio40 group (Figure S1D, S1E, $^{\&\&}P < 0.01$), which were comparable to the Model group. These results further verified that Dio inhibits endothelial cell angiogenesis by targeting α-SMA-mediated EndMT.

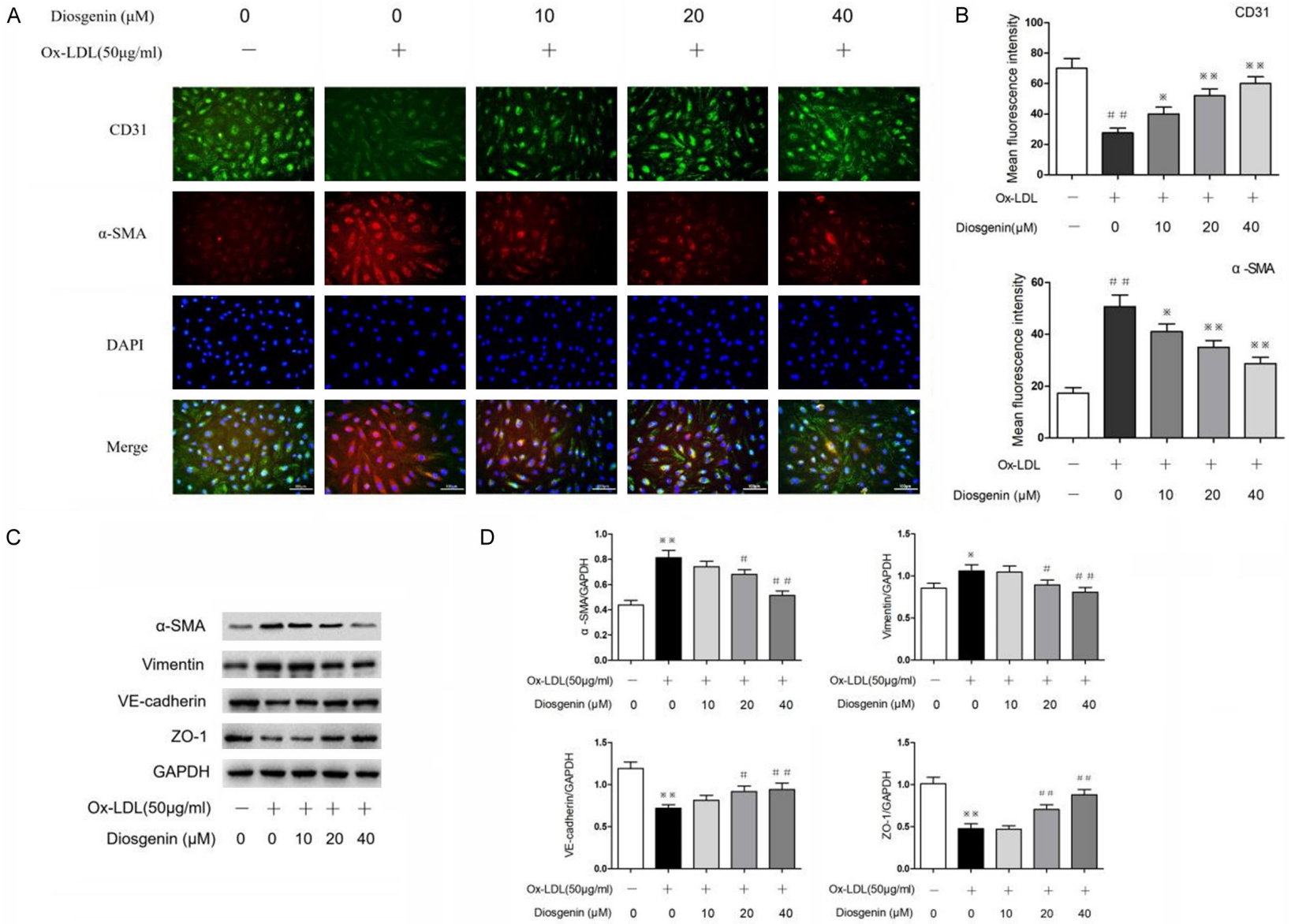

Figure 5. Dio inhibited EndMT in HUVECs stimulated by Ox-LDL. Before Ox-LDL (50 μg/mL) stimulation, HUVECs were treated with 10, 20 and 40 μM Dio for 12 hours. (A) Immunofluorescence was used to detect the expression of CD31 and α-SMA, and (B) The fluorescence intensities of CD31 and α-SMA were measured. (C) Western blot was used to evaluate the expression of α-SMA, vimentin, VE-cadherin and ZO-1 in each group. (D) Quantification of α-SMA, vimentin, VE-cadherin and ZO-1 protein levels. GAPDH was used as an internal control for protein equal loading. Scale bar = 100 μm, Data is expressed as mean ± S.D, n = 3. $^{*}P < 0.05$, $^{**}P < 0.01$ versus the normal group; $^{\#}P < 0.05$, $^{\#\#}P < 0.01$, $^{ns}P \geq 0.05$ versus the model group.

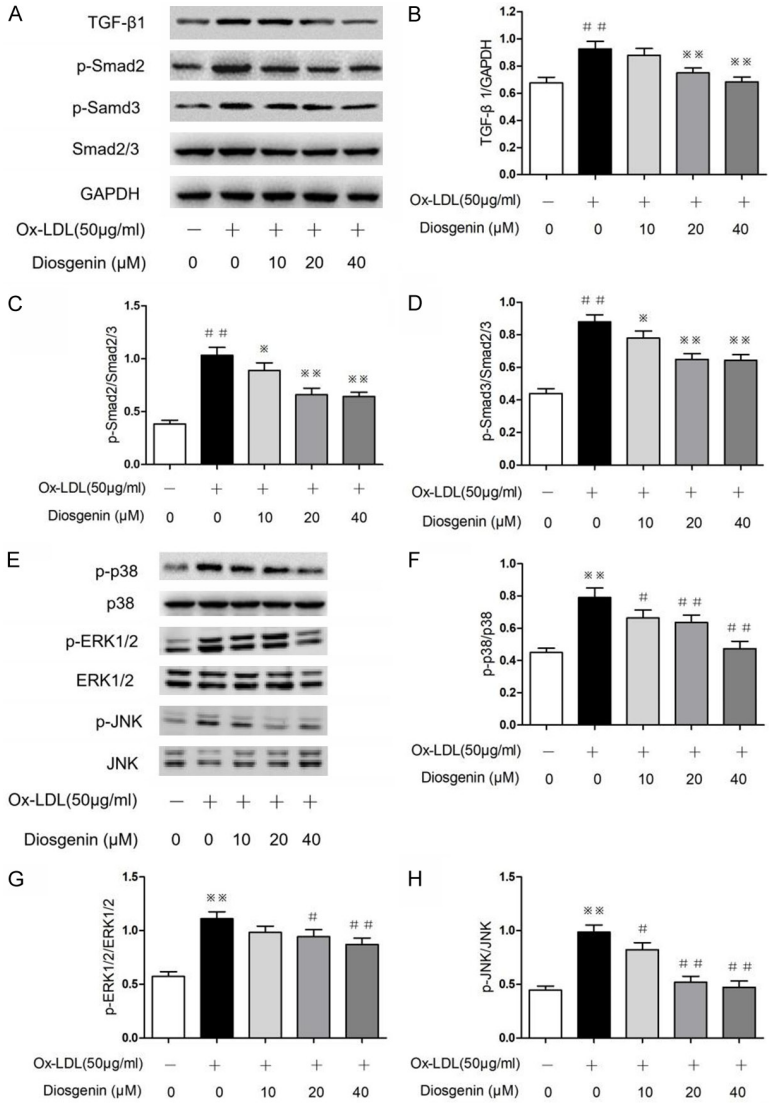

Figure 6. Dio inhibited the activation of TGF-β/Smad and MAPKs signaling pathways in HUVECs stimulated by Ox-LDL. Before Ox-LDL (50 μg/mL) stimulation, HUVECs were treated with 10, 20 and 40 μM Dio for 12 hours. A. Western blot was used to evaluate the expression of TGF-β1, p-Smad2, p-Smad3 and Smad2/3 in each group. B-D. Quantification of TGF-β1, p-Smad2/Smad2/3 and p-Smad3/Smad2/3 protein levels. E. Western blot was used to evaluate the expression of p-p38, p38, p-ERK1/2, ERK1/2, p-JNK and JNK in each group. F-H. Quantification of p-p38/p38, p-ERK1/2/ERK1/2 and p-JNK/JNK protein levels. GAPDH was used as an internal control for protein equal loading. Data is expressed as mean ± S.D, n = 3. $^{**}P < 0.01$ versus the normal group; $^{\#}P < 0.05$, $^{\#\#}P < 0.01$, $^{ns}P \geq 0.05$ versus the model group.

To identify the specific action target of Dio in the TGF-β/Smad signaling pathway, we detected key upstream and downstream molecules. ELISA results showed that Dio concentration-dependently inhibited the secretion of TGF-β1 in HUVECs supernatant (Figure S2A, $^{\#\#}P < 0.01$). Immunofluorescence staining revealed that Ox-LDL stimulation significantly increased TβRI expression, while Dio treatment markedly reduced TβRI levels (Figure S2B, S2C, $^{\#\#}P < 0.01$); however, TβRII expression showed no significant difference among groups (Figure S2B, S2D, $^{ns}P \geq 0.05$), indicating that Dio specifically targets TβRI.

Discussion

A major finding of our research was that the intraperitoneal administration of Dio inhibited the formation and progression of CNV in a laser-induced mouse model. Dio exerted its inhibitory effects on experimental CNV by suppressing the TGF-β/Smad and MAPKs pathways in vivo, thereby reversing the EndMT process. Similarly, in a cellular model mimicking CNV conditions using HUVECs stimulated with Ox-LDL, our data illustrated that Dio inhibited the migration and tubulogenesis capabilities of endothelial cells through the same pathways.

CNV is a distinctive feature of wet AMD, marked by the abnormal growth of new blood vessels in the choroid layer. These freshly-grown vessels are often highly permeable, which can result in the leakage of intraocular fluid and blood [42], which ultimately causes substantial damage to the central vision of those affected. Dio is a natural steroidal saponin primarily derived from yam, which has gained increasing attention for its broad therapeutic effects in multiple health conditions [43]. Recent studies have highlighted Dio's significant activities, including anti-inflammatory [5, 6], antioxidant [7, 44], anti-angiogenesis [45, 46] and anti-fibrotic [9] effects. Its therapeutic potential extends beyond ocular condi-

tions, as emerging evidence indicates that Dio is essential for inhibiting the fibrosis of organs such as liver, kidneys [47] and lungs [9]. Interestingly, a study of Hao Cui indicated that Dio inhibited the expression of endothelial markers VE-cadherin and CD31 in a rat model of ATO-induced myocardial fibrosis, while promoting the expression of mesenchymal cell markers such as α-SMA [34]. Vadivil Dinesh Babu's research showed that Dio could also inhibit EMT by reducing the expression of TGF-β and Smad2/3 signaling proteins in a rat model of BLM-induced pulmonary fibrosis [9]. VEGF is a critical mediator of angiogenic processes in the initiation and progression of CNV [48]. Pin Shan Chen's research has demonstrated that Dio can significantly suppress the angiogenic capacity of endothelial cells by downregulating VEGF expression. Moreover, Dio hinders the phosphorylation of several key proteins known to orchestrate angiogenic key pathways, such as PI3K, ERK and JNK, which lead to its significant antiangiogenic effect [39].

Oxidative stress and inflammation-induced EndMT have emerged as pivotal mechanisms contributing to the pathogenesis of CNV in patients with nAMD [49]. Our comprehensive in vivo and in vitro investigation of EndMT-related proteins aligns with previous findings [16, 50], which reinforces the notion that EndMT signifies the inception of endothelial cell differentiation during angiogenesis [51, 52]. Under oxidative stress and inflammation cues, vascular endothelial cells, which are typically tightly-junctional, undergo a loss of endothelial junction proteins, leading to decreased intercellular adhesion and enhanced migratory capacity. These cells then lose their characteristic cell adhesion properties, undergo cytoskeletal remodeling, and shift from an apical-basal to an anterior-posterior polarity. This morphological change results in spindle-shaped cells with a heightened ability to migrate, which further validates the crucial role of EndMT in CNV pathogenesis [53]. In our research, Dio suppressed the progress of EndMT, which enhanced the hypothetical therapeutic effects of Dio in CNV.

Molecular signaling pathways implicated in CNV development include the activation of TGF-β1, a pleiotropic factor critical to CNV development. Both canonical (Smad) and non-canonical (JNK, p38, ERK 1/2, PI3K/Akt) signaling pathways are mediated by TGF-β1 [54], which regulates cell growth, differentiation, apoptosis, migration and immune responses [36]. TGF-β1 holds a significant position in the context of fibrosis since it activates the fibrotic signaling axis [55, 56]. TGF-β1 binds to its receptors, leading to the phosphorylation of Smad2/3, which then forms a complex with Smad4. This complex translocates into the nucleus, where it activates the transcription of pro-fibrotic genes, such as collagen I, FN1 and α-SMA, resulting in the activation of myofibroblasts, increased extracellular matrix synthesis and decreased degradation [57]. Additionally, TGF-β1 can directly phosphorylate ERK1/2, p38 and JNK upon binding to its receptors. The activation of the MAPKs pathway mediates cellular processes such as inflammation, proliferation, oxidative stress and differentiation, which plays a central role in regulating fibrosis [58-63]. Dio has previously been shown to inhibit angiogenesis by downregulating VEGF expression in PC-3 cells [39]. At a concentration of 10 μmol/L, Dio demonstrated significant inhibitory effects on α-SMA protein expression and effectively counteracting E-cadherin downregulation in high-glucose-treated HK-2 cells [64]. Furthermore, at 100 μM, Dio suppressed the TGF-β1-induced expression of TGF-β receptors I and II in HSC-T6 cells, preventing the phosphorylation of Smad3 [65]. While Dio is known to suppress JNK phosphorylation under several conditions, its effects on the expression of p-ERK1/2 and p-p38 remain controversial and require advanced investigation [39, 66-68].

Our results align with previous studies showing that Dio reduces TGF-β1 expression in laser-induced CNV mouse RPE-choroidal tissues and Ox-LDL-treated HUVECs (Figure S4). Additionally, Dio markedly suppresses the phosphorylation of Smad2 and Smad3, exhibiting both anti-angiogenic and anti-fibrotic effects [65]. In contrast, Chen's study reported that Dio and its derivatives were able to suppress the activation and phosphorylation of JNK in macrophages and microglia induced by LPS, but did not alter the phosphorylation of p38 and ERK1/2 [39]. However, our study observed that Dio notably inhibited the activation and phosphorylation of p38, JNK and ERK1/2 (**Figures 3**, **6F-H**). Potential reasons for these discrepancies may lie in differences in the specific cell types and drug concentrations utilized. Furthermore, while inflammation undoubtedly plays a crucial role in the progression of CNV,

our research findings emphasize the importance of processes such as cellular proliferation, migration and EndMT in CNV pathogenesis.

In conclusion, our study has shown that Dio can significantly reduce laser-induced CNV in mice by suppressing EndMT via the regulation of the TGF-β/Smad and MAPKs signaling cascades. In this experiment, a laser-induced CNV model was employed, utilizing the physical effects of krypton lasers to penetrate the Bruch's membrane and induce an inflammatory response in the local tissues, providing the potential for neovascular growth. However, it could not fully replicate the complexity or diversity of human diseases. Additionally, this study focused on the efficacy of Dio monotherapy and did not explore its synergistic effects combined with other treatments, such as anti-VEGF drugs, which might be an important consideration in actual clinical practices. In summary, although our findings indicate that Dio holds promise as an adjunctive treatment for CNV-related disorders, further in vitro and in vivo research is necessary for translating it into an effective clinical treatment regimen.

Acknowledgements

The authors thank Dr. Tao Kang and Yuan Yuan for their technical help. The study was funded by the National Natural Science Foundation (grant no. 82374214), Changzhou Science and Technology Bureau (CJ20246003) and Jiangsu Provincial Graduate Innovation Project (SJCX25-1005).

Disclosure of conflict of interest

None.

Abbreviations

CNV, Choroidal Neovascularization; AMD, Age-related macular degeneration; nAMD, Neovascular age-related macular degeneration; EndMT, Endothelial-to-Mesenchymal Transition; GA, Geographic atrophy; Dio, Diosgenin; PD, Optic disc; OCT, Optical coherence tomography; FA, Fluorescein angiography; HUVECs, Human Umbilical Vein Endothelial Cells.

Address correspondence to: Xinrong Xu, Department of Ophthalmology, Affiliated Hospital of Nanjing University of Chinese Medicine, No. 155 Hanzhong Road, Qinhuai District, Nanjing 210029, Jiangsu, China. E-mail: yfy133@njucm.edu.cn

References

[1] Arya P and Kumar P. Diosgenin: an ingress towards solving puzzle for diabetes treatment. J Food Biochem 2022; 46: e14390.

[2] Cai B, Zhang Y, Wang Z, Xu D, Jia Y, Guan Y, Liao A, Liu G, Chun C and Li J. Therapeutic potential of diosgenin and its major derivatives against neurological diseases: recent advances. Oxid Med Cell Longev 2020; 2020: 3153082.

[3] Wu S, Zhao M, Sun Y, Xie M, Le K, Xu M and Huang C. The potential of diosgenin in treating psoriasis: studies from HaCaT keratinocytes and imiquimod-induced murine model. Life Sci 2020; 241: 117115.

[4] Li R, Liu Y, Shi J, Yu Y, Lu H, Yu L, Liu Y and Zhang F. Diosgenin regulates cholesterol metabolism in hypercholesterolemic rats by inhibiting NPC1L1 and enhancing ABCG5 and ABCG8. Biochim Biophys Acta Mol Cell Biol Lipids 2019; 1864: 1124-1133.

[5] Mohamadi-Zarch SM, Baluchnejadmojarad T, Nourabadi D, Khanizadeh AM and Roghani M. Protective effect of diosgenin on LPS/D-Gal-induced acute liver failure in C57BL/6 mice. Microb Pathog 2020; 146: 104243.

[6] Binesh A, Devaraj SN and Halagowder D. Atherogenic diet induced lipid accumulation induced NFκB level in heart, liver and brain of Wistar rat and diosgenin as an anti-inflammatory agent. Life Sci 2018; 196: 28-37.

[7] Luo W, Deng J, He J, Yin L, You R, Zhang L, Shen J, Han Z, Xie F, He J and Guan Y. Integration of molecular docking, molecular dynamics and network pharmacology to explore the multi-target pharmacology of fenugreek against diabetes. J Cell Mol Med 2023; 27: 1959-1974.

[8] Corbiere C, Liagre B, Bianchi A, Bordji K, Dauça M, Netter P and Beneytout JL. Different contribution of apoptosis to the antiproliferative effects of diosgenin and other plant steroids, hecogenin and tigogenin, on human 1547 osteosarcoma cells. Int J Oncol 2003; 22: 899-905.

[9] Dinesh Babu V, Suresh Kumar A and Sudhandiran G. Diosgenin inhibits TGF-β1/Smad signaling and regulates epithelial mesenchymal transition in experimental pulmonary fibrosis. Drug Chem Toxicol 2022; 45: 1264-1275.

[10] Liu D, Zhang C, Zhang J, Xu GT and Zhang J. Molecular pathogenesis of subretinal fibrosis in neovascular AMD focusing on epithelial-mesenchymal transformation of retinal pig-

ment epithelium. Neurobiol Dis 2023; 185: 106250.
[11] Lyzogubov VV, Tytarenko RG, Thotakura S, Viswanathan T, Bora NS and Bora PS. Inhibition of new vessel growth in mouse model of laser-induced choroidal neovascularization by adiponectin peptide II. Cell Biol Int 2009; 33: 765-771.
[12] Miller JW, Bagheri S and Vavvas DG. Advances in age-related macular degeneration understanding and therapy. US Ophthalmic Rev 2017; 10: 119-130.
[13] ElSheikh RH, Chauhan MZ and Sallam AB. Current and novel therapeutic approaches for treatment of neovascular age-related macular degeneration. Biomolecules 2022; 12: 1629.
[14] Bloch SB. Implementation studies of ranibizumab for neovascular age-related macular degeneration. Acta Ophthalmol 2013; 91 Thesis7: 1-22.
[15] Comparison of Age-related Macular Degeneration Treatments Trials (CATT) Research Group; Writing Committee, Martin DF, Maguire MG, Fine SL, Ying GS, Jaffe GJ, Grunwald JE, Toth C, Redford M and Ferris FL 3rd. Ranibizumab and bevacizumab for treatment of neovascular age-related macular degeneration: two-year results. Ophthalmology 2020; 127: S135-S145.
[16] Zhang Y, Zhou SQ, Xie MM, Jiang QL, Yang N, Wu R, Zhou J and Xu XR. Licochalcone A alleviates laser-induced choroidal neovascularization by inhibiting the endothelial-mesenchymal transition via PI3K/AKT signaling pathway. Exp Eye Res 2023; 226: 109335.
[17] Li L, Cao X, Huang L, Huang X, Gu J, Yu X, Zhu Y, Zhou Y, Song Y and Zhu M. Lycopene inhibits endothelial-to-mesenchymal transition of choroidal vascular endothelial cells in laser-induced mouse choroidal neovascularization. J Cell Mol Med 2023; 27: 1327-1340.
[18] Chen J, Yang Y, Su S, Zhang S, Huang J, Chen H, Yang X and Sang A. ANGPTL4 promotes choroidal neovascularization and subretinal fibrosis through the endothelial-mesenchymal transition. Int Ophthalmol 2024; 44: 441.
[19] Ishikawa K, Kannan R and Hinton DR. Molecular mechanisms of subretinal fibrosis in age-related macular degeneration. Exp Eye Res 2016; 142: 19-25.
[20] Sun JX, Chang TF, Li MH, Sun LJ, Yan XC, Yang ZY, Liu Y, Xu WQ, Lv Y, Su JB, Liang L, Han H, Dou GR and Wang YS. SNAI1, an endothelial-mesenchymal transition transcription factor, promotes the early phase of ocular neovascularization. Angiogenesis 2018; 21: 635-652.
[21] Medici D, Shore EM, Lounev VY, Kaplan FS, Kalluri R and Olsen BR. Conversion of vascular endothelial cells into multipotent stem-like cells. Nat Med 2010; 16: 1400-1406.
[22] Scott LE, Weinberg SH and Lemmon CA. Mechanochemical signaling of the extracellular matrix in epithelial-mesenchymal transition. Front Cell Dev Biol 2019; 7: 135.
[23] van Meeteren LA, Goumans MJ and ten Dijke P. TGF-β receptor signaling pathways in angiogenesis; emerging targets for anti-angiogenesis therapy. Curr Pharm Biotechnol 2011; 12: 2108-2120.
[24] Orlova VV, Liu Z, Goumans MJ and ten Dijke P. Controlling angiogenesis by two unique TGF-β type I receptor signaling pathways. Histol Histopathol 2011; 26: 1219-1230.
[25] Amin R, Puklin JE and Frank RN. Growth factor localization in choroidal neovascular membranes of age-related macular degeneration. Invest Ophthalmol Vis Sci 1994; 35: 3178-3188.
[26] Pardali E, Goumans MJ and ten Dijke P. Signaling by members of the TGF-beta family in vascular morphogenesis and disease. Trends Cell Biol 2010; 20: 556-567.
[27] Ikushima H and Miyazono K. TGFbeta signalling: a complex web in cancer progression. Nat Rev Cancer 2010; 10: 415-424.
[28] Bian ZM, Elner SG and Elner VM. Regulation of VEGF mRNA expression and protein secretion by TGF-beta2 in human retinal pigment epithelial cells. Exp Eye Res 2007; 84: 812-822.
[29] Suzuki Y, Ito Y, Mizuno M, Kinashi H, Sawai A, Noda Y, Mizuno T, Shimizu H, Fujita Y, Matsui K, Maruyama S, Imai E, Matsuo S and Takei Y. Transforming growth factor-β induces vascular endothelial growth factor-C expression leading to lymphangiogenesis in rat unilateral ureteral obstruction. Kidney Int 2012; 81: 865-879.
[30] Nagineni CN, Samuel W, Nagineni S, Pardhasaradhi K, Wiggert B, Detrick B and Hooks JJ. Transforming growth factor-beta induces expression of vascular endothelial growth factor in human retinal pigment epithelial cells: involvement of mitogen-activated protein kinases. J Cell Physiol 2003; 197: 453-462.
[31] Alvandi Z and Bischoff J. Endothelial-mesenchymal transition in cardiovascular disease. Arterioscler Thromb Vasc Biol 2021; 41: 2357-2369.
[32] Li ZX, Chen JX, Zheng ZJ, Cai WJ, Yang XB, Huang YY, Gong Y, Xu F, Chen YS and Lin L. TGF-β1 promotes human breast cancer angiogenesis and malignant behavior by regulating endothelial-mesenchymal transition. Front Oncol 2022; 12: 1051148.
[33] He J, Sun Y, Jia Y, Geng X, Chen R, Zhou H and Yang B. Ganoderma triterpenes protect against hyperhomocysteinemia induced endothelial-mesenchymal transition via TGF-β signaling inhibition. Front Physiol 2019; 10: 192.
[34] Cui H, Xu W, Liu L, Hong Y, Lou H, Tang P, Lin Y, Xu H, Xie M, Du M, Tang X, Wang Z, Wang Q and

Zhang Y. Diosgenin alleviates arsenic trioxide induced cardiac fibrosis by inhibiting endothelial mesenchymal transition. Phytomedicine 2024; 132: 155891.
[35] Yang SJ, Jo H, Kim JG and Jung SH. Baicalin attenuates laser-induced choroidal neovascularization. Curr Eye Res 2014; 39: 745-751.
[36] Yang F, Sun Y, Bai Y, Li S, Huang L and Li X. Asthma promotes choroidal neovascularization via the transforming growth factor Beta1/Smad signalling pathway in a mouse model. Ophthalmic Res 2022; 65: 14-29.
[37] Feng YF, Yuan F, Guo H and Wu WZ. TGF-β1 enhances SDF-1-induced migration and tube formation of choroid-retinal endothelial cells by up-regulating CXCR4 and CXCR7 expression. Mol Cell Biochem 2014; 397: 131-138.
[38] Zhang HM, Li XH, Chen M and Luo J. Intravitreal injection of resveratrol inhibits laser-induced murine choroidal neovascularization. Int J Ophthalmol 2020; 13: 886-892.
[39] Chen PS, Shih YW, Huang HC and Cheng HW. Diosgenin, a steroidal saponin, inhibits migration and invasion of human prostate cancer PC-3 cells by reducing matrix metalloproteinases expression. PLoS One 2011; 6: e20164.
[40] Cai H, Gong L, Liu J, Zhou Q and Zheng Z. Diosgenin inhibits tumor angiogenesis through regulating GRP78-mediated HIF-1α and VEGF/VEGFR signaling pathways. Pharmazie 2019; 74: 680-684.
[41] Khathayer F and Ray SK. Diosgenin as a novel alternative therapy for inhibition of growth, invasion, and angiogenesis abilities of different glioblastoma cell lines. Neurochem Res 2020; 45: 2336-2351.
[42] Nagai N, Ju M, Izumi-Nagai K, Robbie SJ, Bainbridge JW, Gale DC, Pierre E, Krauss AH, Adamson P, Shima DT and Ng YS. Novel CCR3 antagonists are effective mono- and combination inhibitors of choroidal neovascular growth and vascular permeability. Am J Pathol 2015; 185: 2534-2549.
[43] Chen Y, Tang YM, Yu SL, Han YW, Kou JP, Liu BL and Yu BY. Advances in the pharmacological activities and mechanisms of diosgenin. Chin J Nat Med 2015; 13: 578-587.
[44] Gupta DD, Mishra S, Verma SS, Shekher A, Rai V, Awasthee N, Das TJ, Paul D, Das SK, Tag H, Chandra Gupta S and Hui PK. Evaluation of antioxidant, anti-inflammatory and anticancer activities of diosgenin enriched Paris polyphylla rhizome extract of Indian Himalayan landraces. J Ethnopharmacol 2021; 270: 113842.
[45] Srinivasan S, Koduru S, Kumar R, Venguswamy G, Kyprianou N and Damodaran C. Diosgenin targets Akt-mediated prosurvival signaling in human breast cancer cells. Int J Cancer 2009; 125: 961-967.
[46] Li F, Fernandez PP, Rajendran P, Hui KM and Sethi G. Diosgenin, a steroidal saponin, inhibits STAT3 signaling pathway leading to suppression of proliferation and chemosensitization of human hepatocellular carcinoma cells. Cancer Lett 2010; 292: 197-207.
[47] Chen CT, Wang ZH, Hsu CC, Lin HH and Chen JH. In vivo protective effects of diosgenin against doxorubicin-induced cardiotoxicity. Nutrients 2015; 7: 4938-4954.
[48] Song D, Liu P, Shang K and Ma Y. Application and mechanism of anti-VEGF drugs in age-related macular degeneration. Front Bioeng Biotechnol 2022; 10: 943915.
[49] Wu T, Xu W, Wang Y, Tao M, Hu Z, Lv B, Hui Y and Du H. OxLDL enhances choroidal neovascularization lesion through inducing vascular endothelium to mesenchymal transition process and angiogenic factor expression. Cell Signal 2020; 70: 109571.
[50] Li H, Zhao Q, Chang L, Wei C, Bei H, Yin Y, Chen M, Wang H, Liang J and Wu Y. LncRNA MALAT1 modulates ox-LDL induced EndMT through the Wnt/β-catenin signaling pathway. Lipids Health Dis 2019; 18: 62.
[51] Welch-Reardon KM, Wu N and Hughes CC. A role for partial endothelial-mesenchymal transitions in angiogenesis? Arterioscler Thromb Vasc Biol 2015; 35: 303-308.
[52] Wang SH, Chang JS, Hsiao JR, Yen YC, Jiang SS, Liu SH, Chen YL, Shen YY, Chang JY and Chen YW. Tumour cell-derived WNT5B modulates in vitro lymphangiogenesis via induction of partial endothelial-mesenchymal transition of lymphatic endothelial cells. Oncogene 2017; 36: 1503-1515.
[53] Shu DY, Butcher E and Saint-Geniez M. EMT and EndMT: emerging roles in age-related macular degeneration. Int J Mol Sci 2020; 21: 4271.
[54] Avila-Carrasco L, Majano P, Sánchez-Toméro JA, Selgas R, López-Cabrera M, Aguilera A and González Mateo G. Natural plants compounds as modulators of epithelial-to-mesenchymal transition. Front Pharmacol 2019; 10: 715.
[55] Oruqaj G, Karnati S, Vijayan V, Kotarkonda LK, Boateng E, Zhang W, Ruppert C, Günther A, Shi W and Baumgart-Vogt E. Compromised peroxisomes in idiopathic pulmonary fibrosis, a vicious cycle inducing a higher fibrotic response via TGF-β signaling. Proc Natl Acad Sci U S A 2015; 112: E2048-2057.
[56] Lichtman MK, Otero-Vinas M and Falanga V. Transforming growth factor beta (TGF-β) isoforms in wound healing and fibrosis. Wound Repair Regen 2016; 24: 215-222.
[57] Lamouille S, Xu J and Derynck R. Molecular mechanisms of epithelial-mesenchymal transition. Nat Rev Mol Cell Biol 2014; 15: 178-196.

[58] Hsieh YH, Hung TW, Chen YS, Huang YN, Chiou HL, Lee CC and Tsai JP. In vitro and in vivo anti-fibrotic effects of Fraxetin on renal interstitial fibrosis via the ERK signaling pathway. Toxins (Basel) 2021; 13: 474.
[59] Chen LJ, Xu YL, Song B, Yu HM, Oudit GY, Xu R, Zhang ZZ, Jin HY, Chang Q, Zhu DL and Zhong JC. Angiotensin-converting enzyme 2 ameliorates renal fibrosis by blocking the activation of mTOR/ERK signaling in apolipoprotein E-deficient mice. Peptides 2016; 79: 49-57.
[60] Cheng X, Zheng X, Song Y, Qu L, Tang J, Meng L and Wang Y. Apocynin attenuates renal fibrosis via inhibition of NOXs-ROS-ERK-myofibroblast accumulation in UUO rats. Free Radic Res 2016; 50: 840-852.
[61] Weng CH, Li YJ, Wu HH, Liu SH, Hsu HH, Chen YC, Yang CW, Chu PH and Tian YC. Interleukin-17A induces renal fibrosis through the ERK and Smad signaling pathways. Biomed Pharmacother 2020; 123: 109741.
[62] Wu Y, Wang L, Deng D, Zhang Q and Liu W. Renalase protects against renal fibrosis by inhibiting the activation of the ERK signaling pathways. Int J Mol Sci 2017; 18: 855.
[63] Zhou J, Liu S, Guo L, Wang R, Chen J and Shen J. NMDA receptor-mediated CaMKII/ERK activation contributes to renal fibrosis. BMC Nephrol 2020; 21: 392.
[64] Wang WC, Liu SF, Chang WT, Shiue YL, Hsieh PF, Hung TJ, Hung CY, Hung YJ, Chen MF and Yang YL. The effects of diosgenin in the regulation of renal proximal tubular fibrosis. Exp Cell Res 2014; 323: 255-262.
[65] Xie WL, Jiang R, Shen XL, Chen ZY and Deng XM. Diosgenin attenuates hepatic stellate cell activation through transforming growth factor-β/Smad signaling pathway. Int J Clin Exp Med 2015; 8: 20323-20329.
[66] Choi KW, Park HJ, Jung DH, Kim TW, Park YM, Kim BO, Sohn EH, Moon EY, Um SH, Rhee DK and Pyo S. Inhibition of TNF-α-induced adhesion molecule expression by diosgenin in mouse vascular smooth muscle cells via down-regulation of the MAPK, Akt and NF-κB signaling pathways. Vascul Pharmacol 2010; 53: 273-280.
[67] Jung DH, Park HJ, Byun HE, Park YM, Kim TW, Kim BO, Um SH and Pyo S. Diosgenin inhibits macrophage-derived inflammatory mediators through downregulation of CK2, JNK, NF-kappaB and AP-1 activation. Int Immunopharmacol 2010; 10: 1047-1054.
[68] Cai B, Seong KJ, Bae SW, Chun C, Kim WJ and Jung JY. A synthetic diosgenin primary amine derivative attenuates LPS-stimulated inflammation via inhibition of NF-κB and JNK MAPK signaling in microglial BV2 cells. Int Immunopharmacol 2018; 61: 204-214.

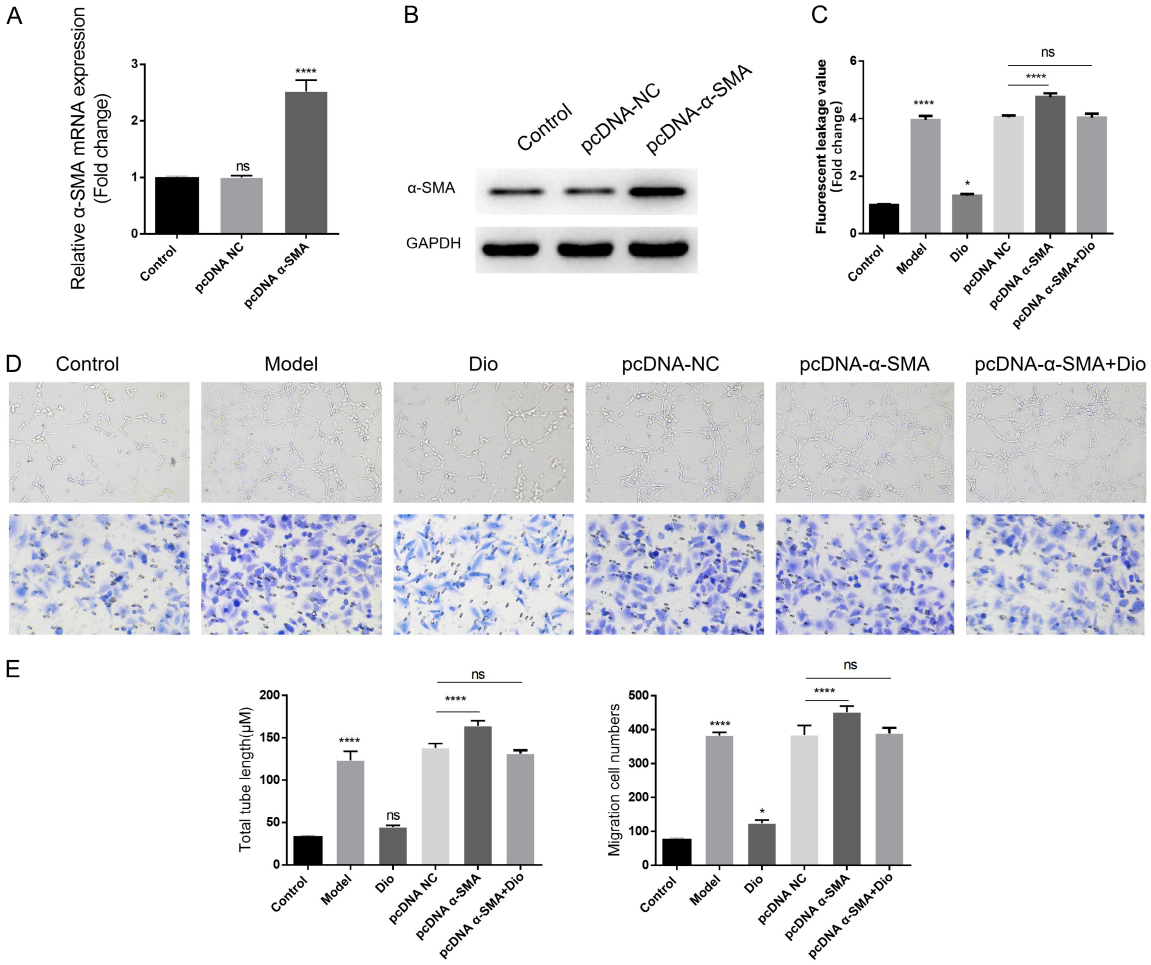

Figure S1. α-SMA overexpression abrogates the inhibitory effects of Diosgenin on EndMT and choroidal neovascularization. Scale bar = 100 μm, $^{*}P < 0.05$, $^{**}P < 0.01$, $^{ns}P \geq 0.05$.

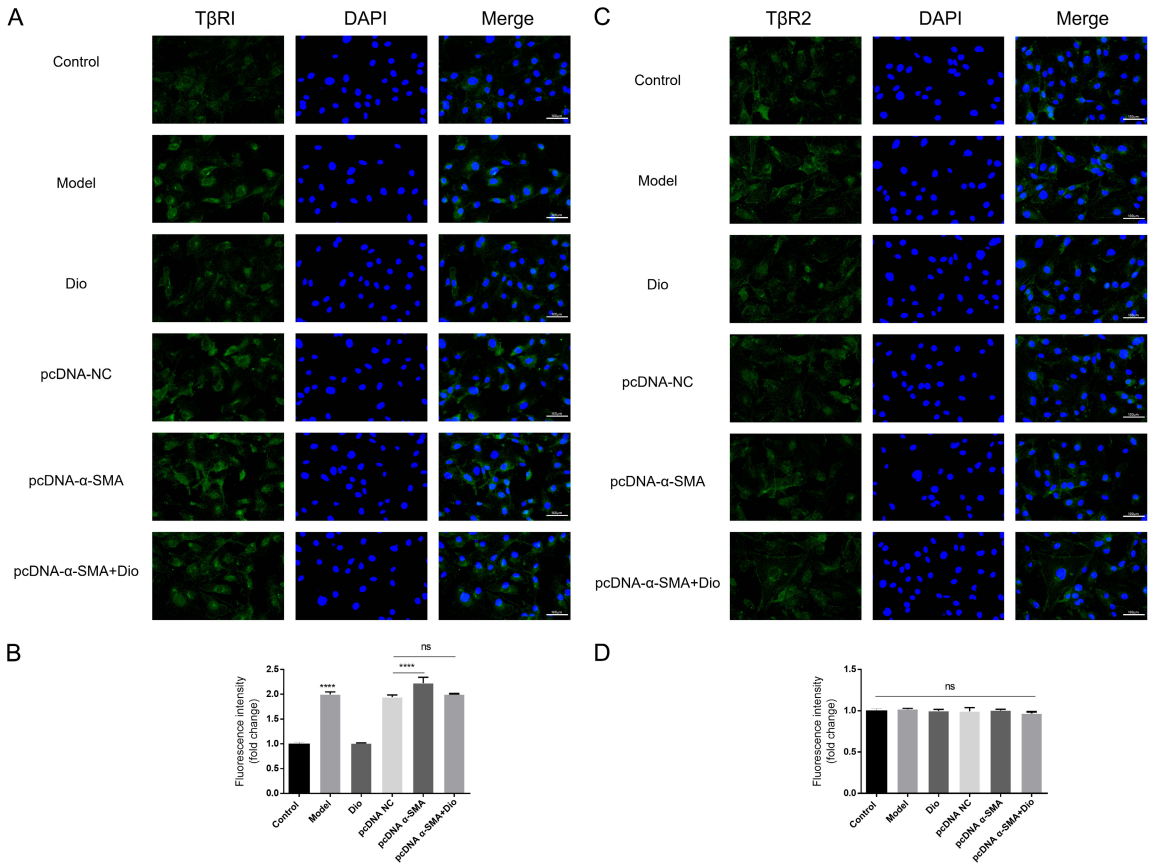

Figure S2. Diosgenin targets TβRI and inhibits TGF-β/Smad signaling at multiple nodes in Ox-LDL-stimulated HUVECs. Scale bar = 100 μm, $^{ns}P \geq 0.05$.

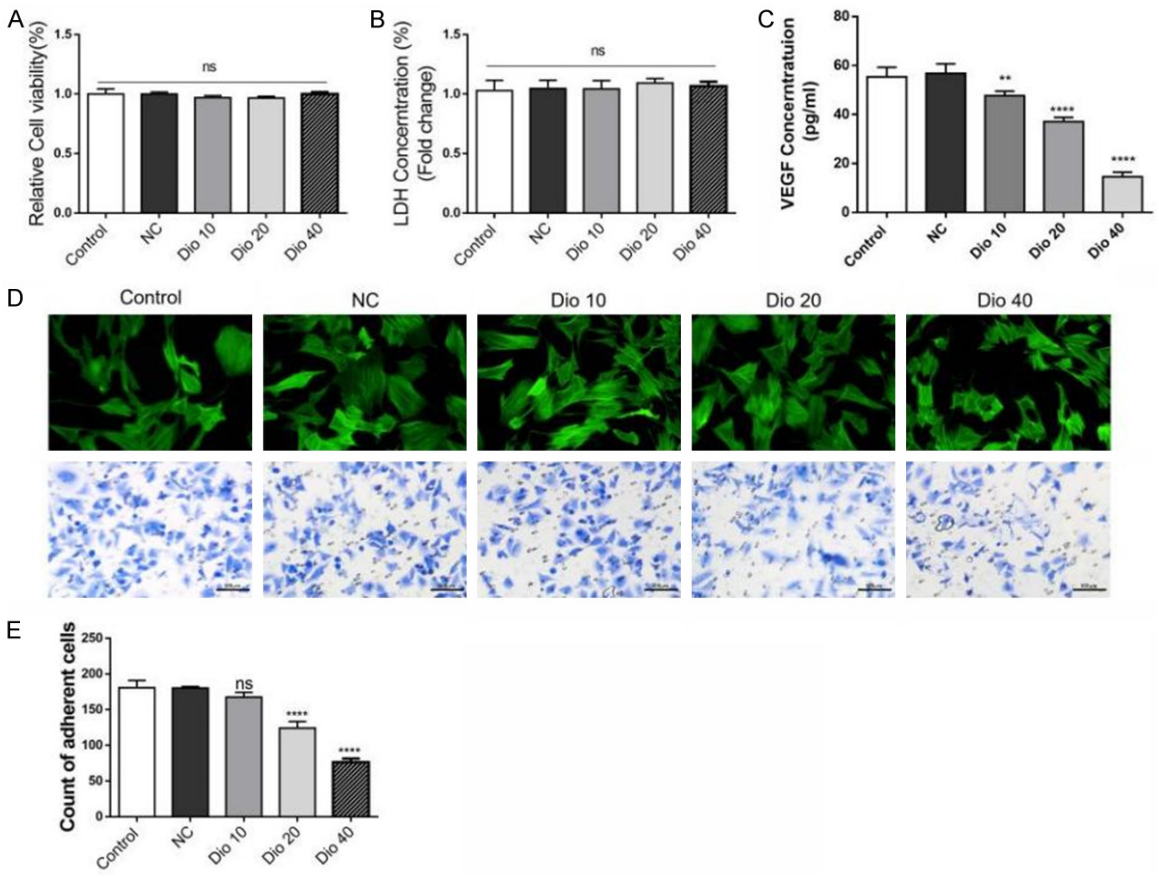

Figure S3. Cytotoxicity exclusion and non-specific inhibition elimination of Dio on HUVECs. Scale bar = 100 μm, $^{*}P < 0.05$, $^{**}P < 0.01$, $^{****}P < 0.0001$, $^{ns}P \geq 0.05$.

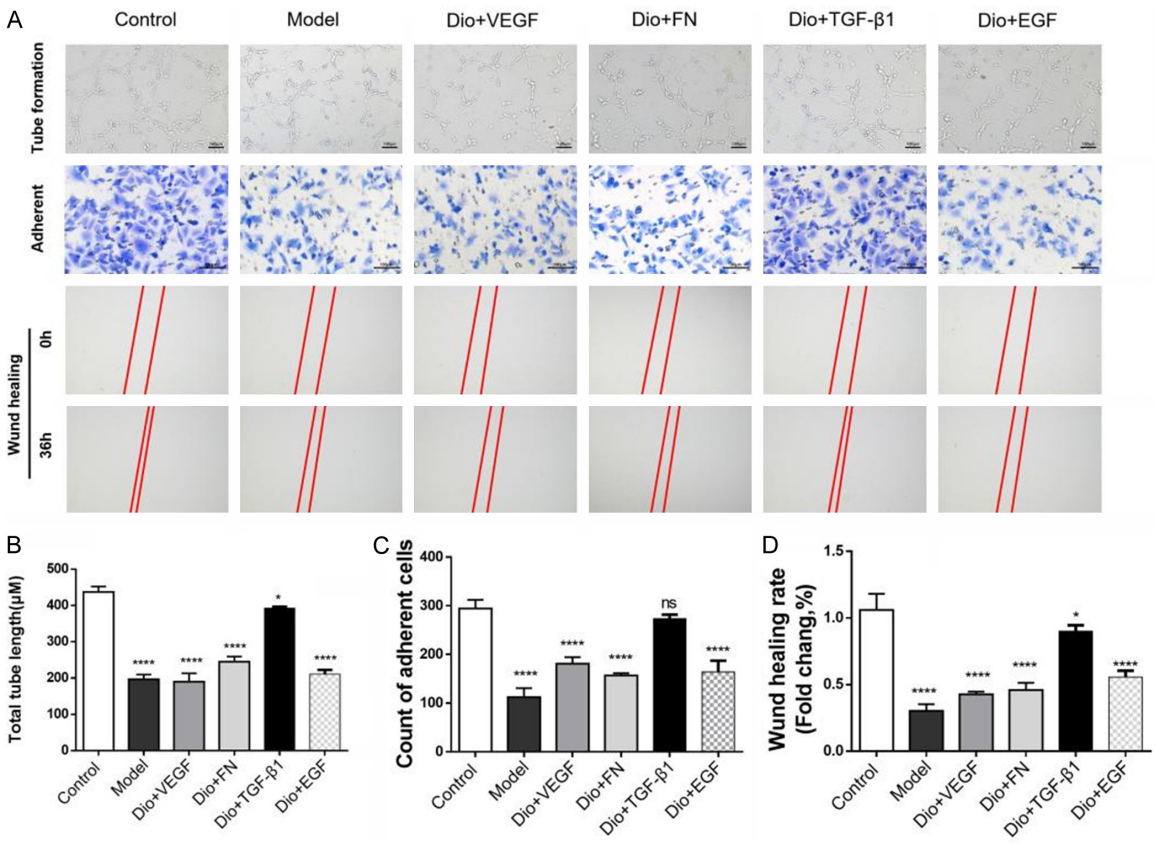

Figure S4. Dio regulates VEGF/VEGFR2 signaling and multi-pathway functional rescue in HUVECs. Scale bar = 100 μm, $^{*}P < 0.05$, $^{**}P < 0.01$, $^{****}P < 0.0001$, $^{ns}P \geq 0.05$.